Hyperpolarization of nuclear spins
Polarization blockade

Whaites, O. T.; Ioannou, C. I.; Pingault, B. J.; Van De Stolpe, G. L.; Taminiau, T. H.; Monteiro, T. S.

DOI
10.1103/PhysRevResearch.5.043291

Publication date
2023

Document Version
Final published version

Published in
Physical Review Research

Editors' Suggestion

Hyperpolarization of nuclear spins: Polarization blockade

O. T. Whaites,[1] C. I. Ioannou,[2,3] B. J. Pingault,[2,3] G. L. van de Stolpe,[2,3] T. H. Taminiau,[2,3] and T. S. Monteiro[1]

[1]*Department of Physics and Astronomy, University College London, Gower Street, London WC1E 6BT, United Kingdom*

[2]*QuTech, Delft University of Technology, P.O. Box 5046, 2600 GA Delft, The Netherlands*

[3]*Kavli Institute of Nanoscience Delft, Delft University of Technology, P.O. Box 5046, 2600 GA Delft, The Netherlands*

(Received 31 August 2023; accepted 19 November 2023; published 26 December 2023)

Efficient hyperpolarization of nuclear spins via optically active defect centers, such as the nitrogen vacancy (NV) center in diamond, has great potential for enhancing NMR-based quantum information processing and nanoscale magnetic resonance imaging. Recently, pulse-based protocols have been shown to efficiently transfer optically induced polarization of the electron defect spin to surrounding nuclear spins—at particular resonant pulse intervals. In this work, we investigate the performance of these protocols, both analytically and experimentally, with the electronic spin of a single NV defect. We find that whenever polarization resonances of nuclear spins are near degenerate with a "blocking" spin, which is single spin with stronger off-diagonal coupling to the electronic central spin, they are displaced out of the central resonant region—without, in general, significant weakening in the rate of polarization. We analyze the underlying physical mechanism and obtain a closed-form expression for the displacement. We propose that spin blocking represents a common but overlooked effect in hyperpolarization of nuclear spins and suggest solutions for improved protocol performance in the presence of (naturally occurring) blocking nuclear spins.

DOI: 10.1103/PhysRevResearch.5.043291

I. INTRODUCTION

There is significant current interest in techniques for the control of nuclear spins using solid-state defects such as nitrogen vacancy (NV) centers in diamond [1,2]. Many of these techniques rely on protocols of periodically applied microwave pulses. Although they were originally developed to dynamically decouple the electron spin from the environment [3–5], it was subsequently found that when pulses are applied at intervals resonant with surrounding nuclear spin precession frequencies, the resulting entanglement between the individual nuclear spin and the electronic spin of the defect offers a very effective technique for sensing and controlling nuclear spin states [1,6,7].

Such pulse-based control has been exploited for nuclear polarization and state initialization with applications ranging from quantum error correction and quantum information [6–11], to nanoscale nuclear magnetic resonance (NMR) and other sensing applications [12,13]. Dynamical nuclear polarization (DNP) [14], i.e., the transfer of polarization from electrons to nuclear spins, originally developed for NMR, is also being developed in this context. Recently proposed pulse-based DNP protocols explicitly aimed at nuclear polarization with NVs, i.e., PulsePol [15] and PolCPMG [16], have been demonstrated to polarize ^{13}C nuclei in diamond. Polarization of spins external to a diamond sample using PulsePol has been achieved using an ensemble of NV centers [17].

However, while these protocols were designed in the setting of polarization transfer to a single nuclear spin, in a realistic setting, the central electronic spin couples to multiple spins. Here we investigate polarization transfer from a central spin to several environmental nuclear spins simultaneously. Polarization transfer to a given nuclear spin occurs efficiently when the DNP protocol period T is near a resonant value

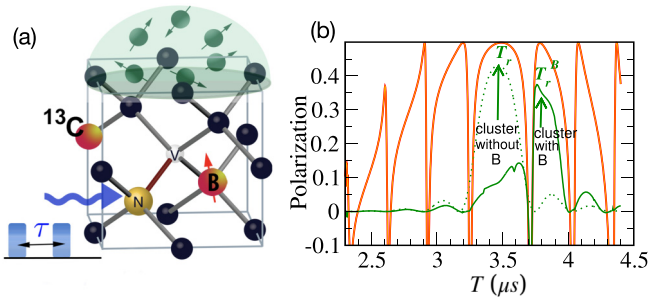

FIG. 1. Illustration of nuclear spin polarization in the presence of a blocking spin. (a) An NV center in diamond. A pulse-based polarization protocol, characterized by a pulse interval τ, is applied to polarize a distant cluster of nuclear spins (in light green). (b) Efficient polarization of the weakly coupled spins (green dots) is expected near the resonant pulse period $T = T_r$. However, in the presence of a nuclear spin that is near degenerate but interacts more strongly with the NV (blocking spin B), the cluster's resonances are displaced, to $T \simeq T_r^B$ (solid green line). The resonance of spin B (red line) is unperturbed. We term this effect "polarization blockade," in analogy to blockade effects encountered in other fields of physics [18].

$T \simeq T_r$, where the nuclear precession frequency becomes resonant with a corresponding protocol frequency. We find such resonant transfer can be suppressed by a blocking spin, i.e., a nuclear spin with similar precession frequency but stronger off-diagonal coupling. This effect is illustrated in Fig. 1: the presence of the blocking spin expels the polarization resonances of the weaker-coupled nuclear spins from the central $T \approx T_r$ region. We analyze the underlying physical mechanism and clarify its relation to dark states, which are known to suppress the polarization of nuclear spins [19,20]. Spin blocking is quite distinct and, to our knowledge, not previously investigated: while dark states suppress polarization by decoupling a subspace of states from the dynamics, spin blocking acts by shifting a subset of spins off resonance. We experimentally verify this analysis using a single NV whose microscopic spin environment has been precisely characterized [21,22].

In Sec. II, we review pulse-based control of nuclear spins and introduce the theoretical Floquet-based models used to analyze the joint dynamics of a central spin and nuclear spins and simulate the experiments. In Sec. III, we present our results in the context of an NV center, including theory-experimental comparisons as well as an expression for the resonance displacement, given by Eq. (6), a key result of the work. In Sec. IV, we discuss the implications for nuclear polarization and more efficient control of nuclear registers.

II. METHODS: PULSE-BASED CONTROL

A central electronic spin surrounded by N_{nuc} nuclear spins may be described by the pure dephasing Hamiltonian, $\hat{H}(t) = \hat{H}_p(t) + \hat{H}_0$, where

$$\hat{H}_0 = \omega_L \sum_{n=1}^{N_{\text{nuc}}} \hat{I}_z^{(n)} + \hat{S}_z \sum_{n=1}^{N_{\text{nuc}}} \mathbf{A}^{(n)} \cdot \hat{\mathbf{I}}^{(n)}. \tag{1}$$

The operators for the electronic spin in a qubit subspace $\{|u\rangle, |d\rangle\}$ and the nuclear spins are labeled $\hat{S}$ and $\hat{I}$, respectively. ω_L is the nuclear Larmor frequency; the hyperfine field $\mathbf{A}^{(n)}$ acting on the nuclear spin has components $A_\perp^{(n)}, A_z^{(n)}$ relative to the z axis; and we take $A_\perp^{(n)} \equiv A_x^{(n)}$, without loss of generality. $\hat{H}_p(t) = \Omega(t)\hat{S}_k$ is the pulse control Hamiltonian in the rotating frame of the microwave field. $\Omega(t)$ is set by the microwave control field, while $k \equiv x, y$ for common protocols.

For pulse-based control, there is a resonant pulse spacing $\tau = \tau_r$ for which the central spin and nuclear spins selectively interact, allowing efficient control of the nuclear states. For example, in the well-known Carr-Purcell-Meiboom-Gill (CPMG) sequence [23], microwave pulses are applied along the x axis at regular intervals, τ; the resonant pulse spacing with a nuclear spin is at $\tau_r^{(n)} = k\pi/\omega_I^{(n)}$, where k is an odd integer and $\omega_I^{(n)} \simeq \omega_L - A_z^{(n)}/2$ for a NV center. For common protocols, the full protocol period T is an integer multiple of τ. For CPMG specifically, it is $T_r = 2\tau_r$. Note that we omit the n superscript for single nuclear spin calculations.

Polarization protocols. Recently, new pulse-based protocols were identified [15,16] which split the electron-nuclear resonance, such that each component selectively addresses one nuclear spin state, allowing polarization. In the present work, we focus on the DNP protocol PulsePol (see Appendix for further details), commonly used due to its robustness to detuning [15]. PulsePol combines a series of x- and y-directional microwave (MW) pulses to map the central spin state onto a nuclear spin. It has pulse period $T = 4\tau$, where τ is the pulse interval. The pulse interval is resonant with a nuclear spin when $\tau_r \simeq k\pi/(4\omega_L)$, for $k = 1, 3 \ldots$, where the third harmonic ($k = 3$) is often selected for its effectiveness [15]. By averaging over the period, an effective, time-independent single nuclear-spin Hamiltonian $\hat{H}^{(n)} \equiv g^{(n)}(\hat{S}_+\hat{I}_-^{(n)} + \hat{S}_-\hat{I}_+^{(n)})$ can be obtained, corresponding to a flip-flop-type interaction between the central spin (S) and the nth nuclear spin (I). The corresponding flip-flop rate at this pulse spacing was found to be $g^{(n)} = A_x^{(n)}(\sqrt{2}+2)/(6\pi)$ [15].

Repetitions. In general, in order to achieve high levels of polarization, repetitions of the polarization protocol are required. For each repetition, N_p cycles are applied a value of τ. This is the periodic component, where the electron-nuclear evolution is largely coherent. However, the central electronic spin is reinitialized after N_p cycles to the $|u\rangle$ state. The reduced nuclear bath evolution is (ideally) uninterrupted. The N_p sequence is then repeated.

A series of central spin reinitializations, interspersed with N_p protocol cycles, is repeated R times. Typically, protocols employ a short run of $N_p = 2$–8 that yields appreciable polarization for strongly coupled nuclear spins with large A_x; if this is followed by many $R \gg 1$ repetitions, polarization of nuclear spins even with weak coupling is gradually achieved. Corresponding theoretical simulations involve R sets of coherent Hamiltonian evolution for $t = 2N_pT$ interspersed with calculation steps where the central spin states are traced out in order to simulate reinitialization.

A. Theoretical methods: Floquet methods

We analyze the coherent dynamics with Floquet theory, a general framework for periodically driven physical systems that has found wide applicability, ranging from NMR continuous driving [24] to pulse-based control of NV centers [25]. However, Floquet theory encompasses several different analytical tools. Floquet engineering (FE) [26] is where a system driven by a typically strong or high-frequency (nonresonant) field can be shown to correspond to an effective, static Hamiltonian with renormalized parameters, by averaging over the period of the driving. Varying the *amplitude* of the nonresonant drive, one may tune over the effective Hamiltonian to induce bath polarization [27]. A common and widely used approach is the Fourier series decomposition of the one-period Hamiltonian, in a suitable rotating frame, which has also been employed for pulse-based control of a nuclear spin bath via a central spin such as an NV center [28]. Floquet spectroscopy [25] has been introduced in this context: resonances for pulse-based protocols were shown to correspond to avoided crossings of the underlying Floquet quasienergies of the pulse-protocol unitary. Thus the morphology of these single or multiple avoided crossings has proved insightful for analysis of electron-nuclear entanglement and polarization in terms of Landau-Zener dynamics [29].

Here we employed both Fourier analysis and Floquet spectroscopy to analyze our results.

Floquet spectroscopy. For a system with a temporally periodic Hamiltonian, $\hat{H}(t+T)=\hat{H}(t)$, Floquet's theorem allows one to write solutions of the Schrödinger equation in terms of quasienergy states, $|\psi_l(t)\rangle = \exp(-i\epsilon_l t)|\Phi_l\rangle$, where ϵ_l is the quasienergy. $|\Phi_l(t)\rangle = |\Phi_l(t+T)\rangle$, where T is the period while $l=1,\ldots,D$ (D is the dimension of the state space).

One may also obtain eigenstates of the one-period unitary evolution operator $\hat{U}(T)\equiv\hat{U}(T,0)$. The Floquet states $|\Phi_l\rangle$ obey the eigenvalue equation,

$$\hat{U}(T)|\Phi_l\rangle = \lambda_l|\Phi_l\rangle \equiv \exp(-i\mathcal{E}_l)|\Phi_l\rangle, \tag{2}$$

where $\mathcal{E}_l(T)\equiv \tan^{-1}\mathrm{Im}\,\lambda_l/\mathrm{Re}\,\lambda_l$ is the eigenphase (the Floquet phase). For Floquet spectroscopy numerics, we diagonalize the full state space of the central spin plus a cluster of $N_{\rm nuc}\sim 1$–7 nuclear spins. Thus we can readily calculate and plot $\mathcal{E}_l(T)$ as a function of period T to investigate resonances and gain insight into the role played here by overlapping avoided crossings.

For Fourier series analysis, a transformation to the toggling frame (the frame of the pulses; see Appendix for details) is widely used, including for analysis of polarization protocols [15,16] and their resonances; a key step is to average over a single period. However, in order to understand experimental traces as a function of τ, we must in addition consider off-resonant behavior (away from $\tau=\tau_r$), as shown below.

The theoretical methods above are applied in the context of a NV center in diamond coupled via the hyperfine interaction to multiple spin-1/2 ^{13}C impurities, although the concepts we present are general. The spin-1 NV is taken in the subspace $\{|u=0\rangle, |d=-1\rangle\}$.

B. Experimental setup

We study the polarization dynamics of nuclear spins surrounding a single NV center at cryogenic temperatures (4 K). The NV electron spin is initialized and read out via resonant optical excitation. The NV sample employed here was previously characterized in detail, allowing for accurate modeling of the microscopic nuclear environment [21,22]. The individual nuclear spins are labeled as C1, C2...,Cn and their hyperfine coupling strengths $A_x^{(n)}, A_z^{(n)}$, taken from [21], are tabulated in the Appendix. The nuclear spin expectation values are read out by applying a combination of nuclear-nuclear and electron-nuclear gates, and subsequently reading out the electron spin state as detailed in [20]. As in previous work [20], we systematically correct for pulse errors and amplitude damping during the readout pulse sequences in order to get a best estimate for the spin expectation values.

III. RESULTS

A. Single-spin polarization: Off-resonant behavior

Details of our analysis are given in the Appendix and here we summarize the key steps. Away from $\tau=\tau_r$, we introduce a small nuclear detuning, slightly altering the PulsePol Hamiltonian to

$$\hat{H}\equiv\sum_{n=1}^{N_{\rm nuc}} g^{(n)}(\hat{S}_+\hat{I}_-^{(n)}+\hat{S}_-\hat{I}_+^{(n)})+\left(\omega_I^{(n)}-\omega\right)\hat{I}_z^{(n)}, \tag{3}$$

where the detuning of each nucleus corresponds to $\delta_n(\tau)=\omega_I^{(n)}-\omega\ll\omega_L$ and the protocol frequency $\omega=3\pi/T=3\pi/(4\tau)$. The resonant nuclear precession frequency is $\omega_I^{(n)}=\sqrt{(\omega_L-A_z^{(n)}/2)^2+(A_x^{(n)}/2)^2}$. For coherent evolution over N_p pulses, we can readily show that the polarization $2\langle\hat{I}_z^{(n)}\rangle$ of a single nuclear spin, for moderate detuning, takes the simple form

$$\mathcal{P}(N_pT)=\left(\frac{2g}{\Omega_r}\right)^2\sin^2\left(\Omega_r N_pT\right), \tag{4}$$

where the generalized Rabi frequency $\Omega_r=\sqrt{\delta^2+(2g)^2}$. Hence, the maximum population transfer into this state is $\mathcal{P}_{\rm max}=1/[1+(\delta/2g)^2]$ at the integer closest to the pulse number $N_p=\pi/(\Omega_r T)$. At resonance, $\delta=0$ and the maximum saturation $\mathcal{P}_{\rm max}=1$. For N_p greater than this maximal value, the polarization oscillates cyclically with Rabi frequency $\Omega_r=2g$. Here, by convention, $\mathcal{P}\in[-1,1]$. We adopt $\mathcal{P}\in[-1/2,1/2]$, where results can be recovered with the appropriate rescaling.

Asymptotic behavior. We note the above result is for a single repetition, $R=1$, and experimental results are in the range $R\sim 10^2$–10^4. One may show that single-spin polarization behavior tends to an asymptotic envelope in the $R\to\infty$ limit. This is illustrated in Fig. 1 (right panel, red solid line). Stronger-coupled spins attain the asymptotic form after a few repetitions. For some weaker-coupled blocked spins, simulations indicate that even $R=10\,000$ may be insufficient to reach the asymptotic limit. A notable feature of the polarization traces is that they exhibit sharp "dips" at period $T=T_{\rm dip}$, seen in Fig. 1 (red solid line) and also seen in the experiments. Here we show that these dips (see Appendix for further details) occur for

$$T_{\rm dip}\simeq\frac{T_r}{(1+\mu^2)}\left[1\pm\frac{n}{3N_p}\sqrt{1+\mu^2\left(\frac{9N_p^2}{n^2}-1\right)}\right], \tag{5}$$

where $n\in\mathbb{Z}^+$, $T_r=6\pi/\omega_I$, and $\mu=2g/\omega_I\ll 1$; thus $T_{\rm dip}\simeq T_r[1\pm\frac{n}{3N_p}]$. The experimental traces also contain additional fine structure due to dephasing arising from the instrumental waiting time $\sim$10 μs in between repetitions.

B. Blockade spins: Theory and experiment

If an NV center has a proximate ^{13}C nuclear spin at a relative orientation, such that the spin has $A_z^B\sim 0$ but reasonably strong off-diagonal coupling A_x^B, then the resonances of weakly coupled spins (with $A_z^s\sim 0$, where $s=1,2,\ldots$) are expelled from the expected resonance region around $T_r=4\tau_r^{(B)}$. We label this spin [see Fig. 1(a)] with superscript B for "blocking" spin. The resonance of the more strongly coupled blocking spin is unperturbed and remains at $T=T_r$, as illustrated in Fig. 1.

Although full numerical simulation of clusters of 5–8 nuclei is feasible, for insight, our analysis of spin blockade requires consideration of the NV electron spin as well as the nuclear spin *pair* comprised of B and one more nuclear spin. This pair dynamics involves the study of an eight-state space. However, two states are largely decoupled and

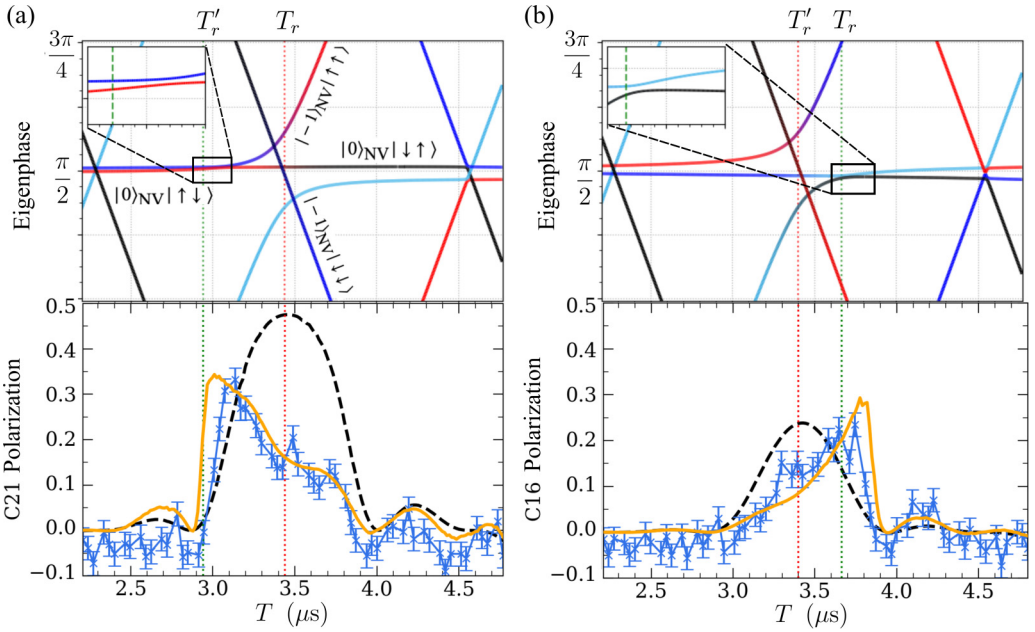

FIG. 2. Comparisons with experiment and spectral analysis. (a) Polarization of weakly coupled nuclear spin C21 with $(A_x, A_z) \equiv (\approx 5.0, -9.7)$ kHz $\times 2\pi$ employing the PulsePol protocol, with $N_p = 2, R = 500$. The NV environment contains a blocking spin C3 with $(A_x^B, A_z^B) \equiv (59., -11.3)$ kHz $\times 2\pi$. Nuclear spin C21 shows the asymmetric displaced resonance expected for $N_p = 2$. Lower panels show experiment (blue), single-spin simulation of C21 (black dashed line), and simulation of C21 and C3 (orange line). The upper panel shows the corresponding Floquet spectra and offers an intuitive spectroscopic understanding of spin blocking. The wide, broad avoided crossing is associated primarily with C3. It overlaps with the much narrower avoided crossing corresponding to the polarization resonance of C21. This means the narrow C21 crossing is pushed away from T_r to *lower* $T_r' < T_r$. (b) For C16, with $(A_x, A_z) \equiv (5.3, -19.8)$ kHz $\times 2\pi$ and $R = 100$, the overlap with the strong C3 avoided crossing results in the narrow C16 crossing being pushed towards larger $T_r' > T_r$. Equation (6) quantifies the magnitude and clarifies that the sign of the displacement depends on $A_z^B - A_z$.

analysis reduces to two triplets of coupled states (numerics involve full diagonalization but, for insight, a simpler model is analyzed).

From Floquet spectroscopy, this scenario corresponds to two sets of avoided crossings in the Floquet eigenphases. One set is illustrated in the upper panels of Fig. 2. It shows the pair of avoided crossings: a very broad crossing of width $\sim A_x^B$ for the case of a strong-coupled spin and, within it, a very narrow crossing due to the weaker-coupled spin since $A_x^B \gg A_x^s$. In other words, the strong avoided crossing involves a pair of states which mostly overlap with states of the single-spin avoided crossing of spin B, while the overlapping narrow crossing involves states that mostly overlap with the weaker spin states.

The lower panels show the corresponding experimental profiles for the weakly coupled nuclear spins C21, with $(A_x, A_z) \equiv (\approx 5.0, -9.7)$ kHz $\times 2\pi$, and C16, with $(A_x, A_z) \equiv (5.3, -19.8)$ kHz $\times 2\pi$, respectively. Their resonances are displaced by the stronger blockade spin C3, which has experimentally measured couplings $(A_z^B, A_x^B) = (-11, -59)$ kHz $\times 2\pi$. There is excellent agreement with simulations. As $N_p = 2$, the resonance takes a characteristic wedge shape, whereas for $N_p = 4$, it is predicted to be fully displaced.

A striking result is that while the C21 resonance is displaced to lower T, for the C16 resonance, the converse is true. Analysis of the three state matrix and its eigenvalues gives the position of the weak spin resonance and magnitude of the displacement (see Appendix for derivation),

$$\Delta T_r / T_r \simeq -\frac{\left(A_x^B\right)^2}{\omega_I^{(s)}\left(\omega_I^{(B)} - \omega_I^{(s)}\right)}. \tag{6}$$

Equation (6) is a key result of this work. Figure 3 tests this expression against numerics and experimental data. In the upper panel, the numerical color map shows polarization as a function of T and detuning $\omega_I^{(B)} - \omega_I^{(s)} \equiv \delta_-$. The overlaid white dots are from Eq. (6) and demonstrate that it provides a robust estimate of the magnitude of the displacement of the polarization resonance peak. The lower panel illustrates an example of the displacement for $N_p = 4$ and spin C16.

In contrast to the observed resonance displacement ΔT_r, the Rabi frequency, or width of the avoided Floquet crossing, is not strongly affected by the blockade spin provided that $|\omega_I^{(B)} - \omega_I^{(s)}|/A_x^B \ll 1$ (see the Appendix for details). In general, the measured polarization is not significantly reduced, but rather shifted to a different period $T_r + \Delta T_r$. There are particular exceptions, such as the case of experimental data for a spin simultaneously perturbed by two blockade spins (discussed in the Appendix).

IV. DISCUSSION

As natural diamond contains of the order of 1.1% of ^{13}C, we estimate that of the order of 20% of NV defects will have a nuclear spin with reasonably strong A_x coupling, but

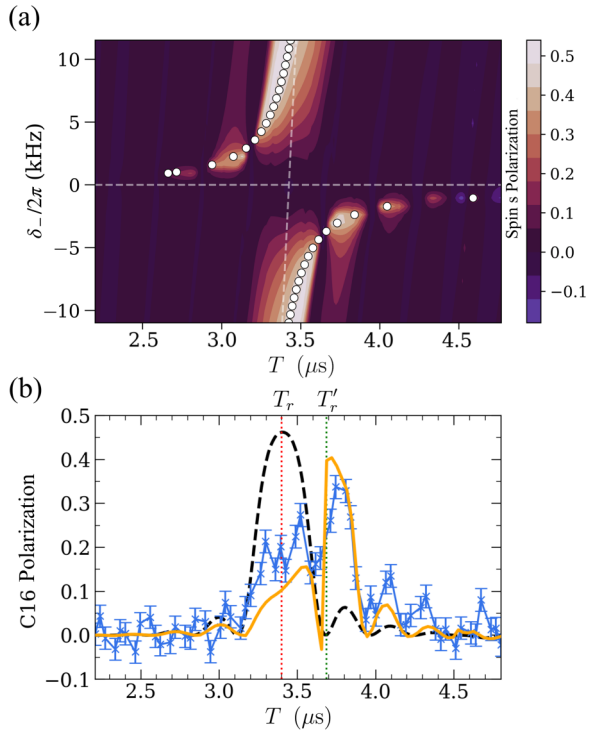

FIG. 3. Upper panel tests the analytical expression for the position of the resonance given by Eq. (6) against numerical simulations, as a function of $\omega_I^{(B)} - \omega_I^{(s)} \equiv \delta_-$. Simulations for this color map use C3 as a blockade spin and spin with $A_x/(2\pi) = 5$ kHz and a variable A_z. Although agreement with the displaced peak is not exact, the expression tracks the displacement quite well. The lower panel compares experimental polarization of C16 (blue) in the presence of blockade spin C3, demonstrating good agreement with simulation (orange) of C3 and C16. For comparison, the undisplaced single C16 simulation is shown (black dashed line). Equation (6) is shown to give reasonable agreement with the displaced peak position. All simulations and experiments in this figure use parameters $N_p = 4$, $R = 100$, which results in a displaced resonance rather than the "wedge" profile obtained for $N_p = 2$.

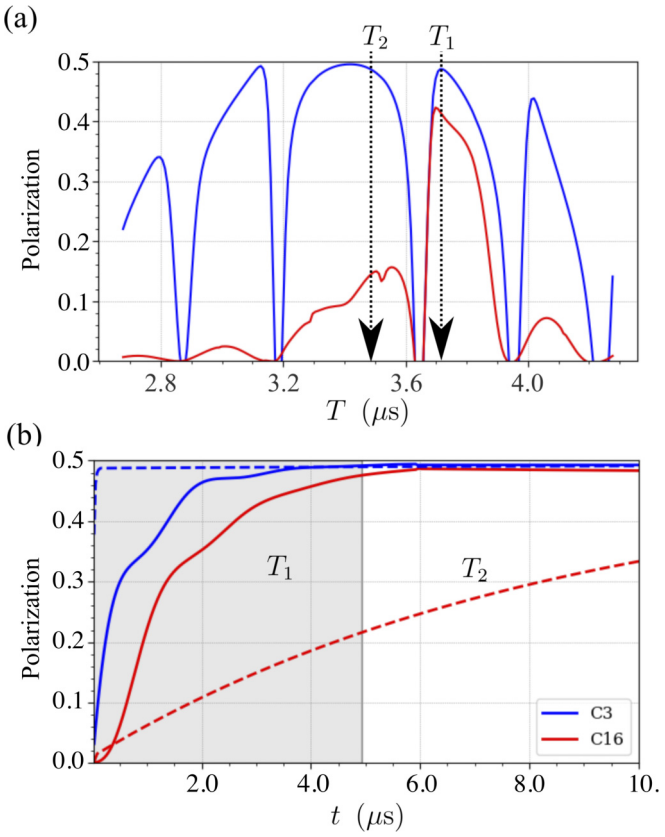

FIG. 4. Compares the conventional polarization method of applying PulsePol at a constant T (or τ) to our proposed adaptation of applying two different regimes of T in the presence of blocking spin C3. (a) Simulated polarization against periodicity of PulsePol, T, with parameters $N_p = 4$, $R = 100$ of both C3 in blue and C16 in red. The two regimes are highlighted as $T_1 \simeq T_r + \Delta T_r \simeq 3.70$ µs, which is a periodicity at the displaced resonance, and $T_2 \simeq T_r \simeq 3.48$ µs near the original resonance. (b) Simulations of the polarization of both spins as a function of increasing total time. The solid line is the application of 200 repetitions (gray region) at T_1, followed by 200 repetitions at T_2; the dashed line is the application of 400 repetitions at T_2. A higher level of polarization in less time is achieved for C16. For the polarization of C3, although polarization rises rapidly for both values of T, driving close to its resonant value at $T = T_2$, rather than far off resonance at $T = T_1$, is important for ensuring robust polarization, to the 0.5 limit.

with $A_z \sim 0$, and thus is able to produce a blocking effect on distant, weakly coupled nuclear spins.

However, Eq. (6) makes clear that the blocking effect is more generic and will occur wherever a weaker-coupled spin is near degenerate with a stronger-coupled spin, and thus can occur for arbitrary A_x, A_z, provided $A_x^{(B)} \gg A_x$ and $A_z^{(B)} \sim A_z$. Thus it should be a relatively common feature in such studies and spin blocking is identifiable via its distinctive spectral profiles, such as the "wedge" shape for $N_p = 2$. The scenario of two blocking spins acting simultaneously on a weaker spin is less common; but in the present data, we observed the case where two blocking spins act to provide displacements of opposite signs (presented in the Appendix). The result is a sort of destructive cancellation that fully suppresses the resonance peak of the weaker spin. While the present study considered PulsePol, our simulations show that similar behavior also occurs for PolCPMG.

An understanding of the blocking spin mechanism allows one to propose approaches to improve the polarization of weak spins. Figure 4 demonstrates a method for drastically improving the polarization efficiency by employing two different T. The upper panel highlights the shifted resonance of spin C16 in the presence of blockade spin C3. First, PulsePol is applied with $T \simeq T_r + \Delta T_r$ in the region with the shifted resonance to polarize weak spins. Following this, PulsePol with $T \simeq T_r$ is applied to maximize polarization: the asymptotic, saturated polarization is maximal for $T \simeq T_r$. The lower panel compares the effectiveness of the two T methods compared to the standard technique of applying the protocol at $T = T_r$ only. The two-spin system of C16 (weak spin) and C3 (blocking spin) was used. The initial stage (gray region) with $T \simeq T_r + \Delta T_r$ shows rapid polarization of both spins (solid lines); the second stage with $T \simeq T_r$ then yields an improvement on overall polarization relative to the single T, on-resonance polarization (dashed line).

Spin-blocking effects are relevant to DNP of ^{13}C in the diamond crystal and, potentially, external nuclear spins as well. Even for different spin species with different Larmor frequencies, accidental resonances [30] such as those that occur between harmonics for ^{1}H and ^{13}C might come into play, but this has not been investigated here.

Spin blocking versus dark modes. Dark-bright modes are an ubiquitous effect occurring in the physics of three-level systems [31,32]: if we consider two degenerate modes, with eigenvalues $\epsilon_{1,2} \approx \epsilon$, independently interacting with a third mode $\epsilon_3 \sim \epsilon$ with finite coupling strengths $g_1 = g_2 \equiv g$, but not with each other, then modes 1,2 hybridize such that one of the hybrid modes fully decouples from mode 3 (dark mode, effective $g = 0$) while the others acquire enhanced coupling $\sqrt{2}g$ (bright modes). The spectral signature is generic [31]: instead of two independent avoided crossings of width g_1 and g_2, the mixing/hybridization produces a single wider avoided crossing of width $\sqrt{2}g$ and a completely decoupled state. The role of dark states in impeding polarization has been noted [20] and investigated in a many-body context [27].

Spin blocking is a distinct polarization suppression mechanism. It occurs for similar regimes, but for the case where the coupling is highly anisotropic, $g_1 \gg g_2$. The spectral signature is also generic. There are, once again, two separate crossings, of width not far from the unperturbed widths g_1 and $\sim g_2$, like the unhybridized case. However, only mode 1 remains at $\epsilon \simeq \epsilon_1$. The weaker-coupled mode has its crossing pushed out of the $\epsilon \approx \epsilon_{1,2}$ region. For the polarization protocols, the weaker spin in effect is pushed off resonance, which is different from having the effective coupling suppressed, as is the case for a dark state.

Off-resonant driving, in general, does not fully suppress polarization and, in principle, all spins should eventually tend to the $R \to \infty$ limit, which is only maximal on resonance. However, it may make it extremely inefficient and slow, potentially allowing imprecisions and decoherent processes to perturb the protocol in a real experiment. However, unlike dark-mode suppression, the effect may be mitigated by adjusting the protocol period to account for the shifted resonance.

V. CONCLUSIONS

In conclusion, in the present work, we introduce, and theoretically and experimentally investigate, the spin-blockade effect, thus named in analogy to blockade effects [18] encountered in other fields of physics. We show that nuclear spins with strong interactions to the central spin can block polarization transfer by detuning weaker-coupled spins away from resonance. This many-body effect, detrimental for polarization efficiency, can be mitigated by pulse sequences that are tailored to the microscopic configuration of the spin system. Polarization transfer to a complex spin system can be highly dependent on the microscopic configuration of the spins and our results thus provide an opportunity for optimization of dynamical nuclear polarization in various settings.

ACKNOWLEDGMENTS

O.W. acknowledges support from an EPSRC DTP grant. This work was supported by the Netherlands Organization for Scientific Research (NWO/OCW) through a Vidi grant. This project has received funding from the European Research Council (ERC) under the European Union's Horizon 2020 research and innovation programme (Grant Agreement No. 852410). This work is part of the research programme NWA-ORC (Grants No. NWA.1160.18.208 and No. NWA.1292.19.194), (partly) financed by the Dutch Research Council (NWO). This work was supported by the Dutch National Growth Fund (NGF), as part of the Quantum Delta NL programme. We acknowledge funding from the Dutch Research Council (NWO) through the project "QuTech Phase II funding: Quantum Technology for Computing and Communication" (Project No. 601.QT.001). B.P. acknowledges financial support through a Horizon 2020 Marie Sklodowska-Curie Actions global fellowship (COHESiV, Project No. 840968) from the European Commission. We thank M. Markham and D. J. Twitchen from Element Six for providing the diamond.

APPENDIX A: NUCLEAR SPIN PARAMETERS

1. PulsePol polarization protocol

In this Appendix, we briefly review the well-studied PulsePol protocol. Consider a nitrogen vacancy (NV) defect in diamond coupled to N_{nuc} ^{13}C spins in a global magnetic field, B_0. Under a microwave control field, the pure dephasing Hamiltonian in the rotating frame of the NV is

$$\hat{H}(t) = \left[\omega_L \hat{I}_z^{(n)} + \hat{S}_z\left(A_z^{(n)}\hat{I}_z^{(n)} + A_x^{(n)}\hat{I}_x^{(n)}\right)\right] + \Omega(t)\hat{S}_{\varphi(t)}, \quad \text{(A1)}$$

for a single (nth) nuclear spin and where $\omega_L = -\gamma_C B_0$ with a nuclear gyromagnetic ratio γ_C, $A_i^{(n)}$ are ith components of the hyperfine coupling strength relative to the z axis between the n th nuclei to the NV, $\Omega(t)$ is the waveform of the microwave control field, $\hat{S}_i$ are in the qubit basis $m_s = \{0, -1\}$, $\hat{I}_i^{(n)}$ are the nth nuclear spin-1/2 operators, and $\hat{S}_{\varphi(t)} = \cos[\varphi(t)]\hat{S}_x + \sin[\varphi(t)]\hat{S}_y$. The experimental external magnetic field strength is aligned with the NV z axis and measured to be $B_0 = 403$ G. The derivation of this Hamiltonian has assumed the rotating wave approximation. For brevity, we assume $\hbar = 1$ in this Appendix, unless considering experimental results in SI units.

The waveform of the microwave control field is dependent on the dynamical decoupling (DD) protocol that is applied. PulsePol is a DD protocol used for dynamic nuclear polarization (DNP), as it is state selective. The form of this pulse protocol is $[(\frac{\pi}{2})_Y\ \tau\ (\pi)_{-X}\ \tau\ (\frac{\pi}{2})_Y (\frac{\pi}{2})_X\ \tau\ (\pi)_Y\ \tau\ (\frac{\pi}{2})_X]^{2N_p}$, where $(\theta)_\varphi$ is a pulse with duration $T_p = \theta/\Omega$ with phase φ, and pulse spacing τ is free evolution. The Rabi frequency due to the microwave drive is denoted Ω. This protocol is periodic with period $T = 4\tau$ and it is applied for a total time of $T_{\text{tot}} = 8N_p\tau$. Using the waveform of the DD control field, the system can be transformed into the frame of the microwave control field, also known as the toggling frame, such that the Hamiltonian in this frame is

$$\hat{H}(t) = \left\{\omega_I^{(n)}\hat{I}_z^{(n)} + [f_1(t)\hat{S}_x + f_2(t)\hat{S}_y](A_z^{(n)}\hat{I}_z^{(n)} + A_x^{(n)}\hat{I}_x^{(n)})\right\}, \quad \text{(A2)}$$

where $f_i(t)$ are known as the modulation functions with period $f_i(t+2T) = f_i(t)$ and are step functions of the form

$$f_1(t) = \begin{cases} 1 \text{ for } 0 < t < \tau \text{ and } 5\tau < t < 6\tau \\ -1 \text{ for } \tau < t < 2\tau \text{ and } 4\tau < t < 5\tau \\ 0 \text{ otherwise} \end{cases} \tag{A3}$$

and

$$f_2(t) = \begin{cases} 1 \text{ for } \tau < t < 3\tau \text{ and } 7\tau < t < 8\tau \\ -1 \text{ for } 3\tau < t < 4\tau \text{ and } 6\tau < t < 7\tau \\ 0 \text{ otherwise.} \end{cases} \tag{A4}$$

These functions are periodic and so a Fourier decomposition can be used, where, for $f_1(t)$,

$$f_1(t) = \sum_{k=0}^{\infty} \left[a_k^{(1)} \cos\left(\frac{k\pi t}{4\tau}\right) + b_k^{(1)} \sin\left(\frac{k\pi t}{4\tau}\right) \right], \tag{A5}$$

where

$$\begin{aligned} a_k^{(1)} &= \frac{1}{k\pi} \frac{1-(-1)^k}{2} \left[4\sin\left(\frac{k\pi}{4}\right) - 2\sin\left(\frac{k\pi}{2}\right) \right], \\ b_k^{(1)} &= \frac{1}{k\pi} \frac{1-(-1)^k}{2} \left[-4\cos\left(\frac{k\pi}{4}\right) + 2 \right], \end{aligned} \tag{A6}$$

and the remaining modulation function $f_2(t)$ can be found in a similar fashion, only with coefficients $a_k^{(2)} = -(-1)^{\frac{2k-2}{4}} b_k^{(1)}$ and $b_k^{(2)} = (-1)^{\frac{2k-2}{4}} a_k^{(1)}$ due to the shift of $t - 2\tau$ in their time dependence. If it is assumed that $A_x << \pi/\tau$, then the time dependence of the Hamiltonian can be resolved in a perturbative fashion using the Magnus expansion. To first order, the evolution operator is $\hat{U}(2T) = \exp[-i2\hat{H}_{\text{avg}}T]$, where $\hat{H}_{\text{avg}}$ is the time period averaged Hamiltonian constructed as

$$\hat{H}_{\text{avg}} = \frac{1}{2T} \int_0^{2T} \hat{H}(t)\, dt, \tag{A7}$$

hence removing the time dependence in place of time averaged field strengths. This assumption of small timescales is fulfilled by transforming into the interaction frame of the nuclear spin of interest and assuming that $A_x \ll 1/T$. Choosing the resonance $\tau_r \simeq 3\pi/(4\omega_L)$ or $k = 3$, and taking the time average for the first-order perturbation, the first-order Hamiltonian can be found to be

$$\hat{H}_{\text{avg}} = \sum_{n=1}^{N_{\text{nuc}}} \left[g^{(n)} (\hat{S}_+ \hat{I}_-^{(n)} + \hat{S}_- \hat{I}_+^{(n)}) + \delta^{(n)} \hat{I}_z^{(n)} \right], \tag{A8}$$

where we assume the Hamiltonian is an independent sum of N_{nuc} spins, with all interactions mediated by the central electronic spin. We define $g^{(n)} = A_x^{(n)}\alpha/4$, $\alpha = 2(\sqrt{2}+2)/3\pi$, and $\delta^{(n)} = \omega_I^{(n)} - \omega_p$ ($\simeq A_z^{(n)}/2$ for $\omega_p = 3\pi/T \simeq \omega_L$) and resonance harmonic k. For simplicity, as stated previously, $k = 3$ is chosen and will be absorbed into the relationship between protocol frequency and period, such that $\omega_p = k\pi/T = 3\pi/T$. The nuclear precession frequency is $\omega_I^{(n)} = \sqrt{(\omega_L - A_z^{(n)}/2)^2 + (A_x^{(n)}/2)^2}$. This Hamiltonian is appropriate for small detuning from the nuclear precession frequency, or that $|\delta| \ll \omega_L$. If this is not satisfied, higher-order terms may be needed.

APPENDIX B: SINGLE-SPIN POLARIZATION

We now review the simplest case of a NV center and a single nuclear spin. While this is well known, it is important for our study to keep track of the detuning δ as we are interested in the behavior away from the resonant pulse period. Equation (A8), for the case of a single spin, takes the matrix form

$$\hat{H}_{\text{avg}} = \begin{matrix} \\ |\uparrow\uparrow\rangle \\ |\downarrow\uparrow\rangle \\ |\uparrow\downarrow\rangle \\ |\downarrow\downarrow\rangle \end{matrix} \begin{matrix} \begin{matrix} |\uparrow\uparrow\rangle & |\downarrow\uparrow\rangle & |\uparrow\downarrow\rangle & |\downarrow\downarrow\rangle \end{matrix} \\ \begin{pmatrix} \delta/2 & 0 & 0 & 0 \\ 0 & \delta/2 & g & 0 \\ 0 & g & -\delta/2 & 0 \\ 0 & 0 & 0 & -\delta/2 \end{pmatrix} \end{matrix}, \tag{B1}$$

where the superscript in the previous section is removed in the single-spin case for simplicity. For ease of notation, the NV states are relabelled as $|0/-1\rangle = |\uparrow/\downarrow\rangle$.

From this, we see that the stretched states are decoupled as follows:

$$|\Phi_1\rangle = |\uparrow\uparrow\rangle, \quad \epsilon_1 = \delta/2, \tag{B2}$$

$$|\Phi_2\rangle = |\downarrow\downarrow\rangle, \quad \epsilon_2 = -\delta/2, \tag{B3}$$

while the antialigned states form a 2×2 subspace of $\{|\uparrow\downarrow\rangle, |\downarrow\uparrow\rangle\}$, or a pseudospin-1/2 Hamiltonian of the form

$$\hat{H} = \delta \hat{I}_z + 2g\hat{I}_x = \mathbf{h}\cdot\hat{\mathbf{I}}, \tag{B4}$$

where $\mathbf{h} = \omega(\sin\theta_p, 0, \cos\theta_p)$ with eigenstates and eigenvalues,

$$\begin{aligned} |\Phi_3\rangle &= \cos\left(\frac{\theta_p}{2}\right)|\downarrow\uparrow\rangle + \sin\left(\frac{\theta_p}{2}\right)|\uparrow\downarrow\rangle, \quad \epsilon_3 = \frac{\omega}{2}, \\ |\Phi_4\rangle &= \sin\left(\frac{\theta_p}{2}\right)|\downarrow\uparrow\rangle - \cos\left(\frac{\theta_p}{2}\right)|\uparrow\downarrow\rangle, \quad \epsilon_4 = -\frac{\omega}{2}, \end{aligned} \tag{B5}$$

defining $\omega = \sqrt{\delta^2 + 4g^2}$ and $\tan\theta_p = 2g/\delta$. The detuning from the nuclear resonance creates an effective magnetic field in this subspace which is not aligned with the x axis. This misalignment reduces the maximum transfer between these two states. To see this, consider an initial state of $|\psi(0)\rangle = |\uparrow\downarrow\rangle$. With the unitary $\hat{U}(t) = \exp(-i\hat{H}_{\text{avg}}t)$ and $|\psi(t)\rangle = \hat{U}(t)|\psi(0)\rangle$, we readily obtain

$$\begin{aligned} |\psi(T_{\text{tot}} = 2N_pT)\rangle = \{&\cos[\varphi(T_{\text{tot}})] + i\cos(\theta_p)\sin[\varphi(T_{\text{tot}})]\} \\ &\times |\uparrow\downarrow\rangle - i\sin(\theta_p)\sin[\varphi(T_{\text{tot}})]|\downarrow\uparrow\rangle, \end{aligned} \tag{B6}$$

where $\varphi(t) = \omega t/2$. The population from the $|\uparrow\downarrow\rangle$ state will transfer into the corresponding flip-flop state $|\downarrow\uparrow\rangle$. The population in this state is then

$$P_{\downarrow\uparrow}(T_{\text{tot}}) = |\langle\downarrow\uparrow|\psi(T_{\text{tot}})\rangle|^2 = \sin^2(\theta_p)\sin^2\left(\omega N_pT\right), \tag{B7}$$

and hence the maximum population transfer into this state is $P_{\downarrow\uparrow}^{\max} = \sin^2\theta_p = 1/[1+(\delta/2g)^2]$ at $N_p = \pi/(\omega T)$. On resonance, or $\delta = 0$, the maximum saturation $P_{\downarrow\uparrow}^{\max} = 1$, as expected. The system undergoes oscillations between these two states characterized by the frequency $\Omega_r = \omega = \sqrt{\delta^2 + 4g^2}$, the generalized Rabi frequency.

1. Mixed states and repetitions

In general, nuclear spins such as ^{13}C are not naturally in a pure state, but instead are in a thermal mixture of equal parts $|\uparrow\rangle$ and $|\downarrow\rangle$. This is often represented as a density matrix, where the thermal mixture is initially

$$\rho_I(0) = \frac{1}{2}\begin{matrix}|\uparrow\rangle \\ |\downarrow\rangle\end{matrix}\begin{pmatrix}1 & 0 \\ 0 & 1\end{pmatrix} = \frac{\rho_\uparrow}{2} + \frac{\rho_\downarrow}{2}. \tag{B8}$$

However, the NV is initialized into one of the basis states, where here it is taken that the NV is initialized into the $|\uparrow\rangle$ state such that $\rho_{\rm NV}(0) = \rho_\uparrow$. As with the state representation, the density matrix of the product space of NV-C is constructed through the tensor product $\rho(0) = \rho_{\rm NV}(0) \otimes \rho_{\rm I}(0)$. The initial density matrix then evolves in time according to the transformation

$$\rho(T_{\rm tot}) = \hat{U}(T_{\rm tot})\,\rho(0)\,\hat{U}^\dagger(T_{\rm tot}). \tag{B9}$$

For this system, the evolved density matrix is found to be

$$\rho(T_{\rm tot}) = \tfrac{1}{2}$$
$$\begin{matrix}|\uparrow\uparrow\rangle \\ |\downarrow\uparrow\rangle \\ |\uparrow\downarrow\rangle \\ |\downarrow\downarrow\rangle\end{matrix}\begin{pmatrix}1 & 0 & 0 & 0 \\ 0 & |\beta(T_{\rm tot})|^2 & \alpha^*(T_{\rm tot})\beta(T_{\rm tot}) & 0 \\ 0 & \alpha(T_{\rm tot})\beta^*(T_{\rm tot}) & |\alpha(T_{\rm tot})|^2 & 0 \\ 0 & 0 & 0 & 0\end{pmatrix}, \tag{B10}$$

where $\alpha(t) = \cos[\varphi(t)] + i\cos(\theta_p)\sin[\varphi(t)]$ and $\beta(t) = -i\sin(\theta_p)\sin[\varphi(t)]$. In order to simplify this and explicitly show the evolution of the ^{13}C spin, a partial trace can be performed on this density matrix in order to reduce the 4×4 matrix to a 2×2 matrix and trace out the NV states. A partial trace over one subspace, $\mathcal{H}_B$, with basis states $\{|b_l\rangle\}$ in a dual system between this subspace and $\mathcal{H}_A$ with basis states $\{|a_i\rangle\}$ is defined as

$$\rho_A = {\rm tr}_B(\rho_{AB}) = \sum_{ijlk} c_{ijlk}|a_i\rangle\langle a_j|\langle b_l|b_k\rangle, \tag{B11}$$

where the dual-space density matrix is decomposed as $\rho_{AB} = \sum_{ijlk} c_{ijlk}|a_i\rangle\langle a_j| \otimes |b_l\rangle\langle b_k|$. By performing this operation over the NV basis states on the full density matrix in Eq. (B10), the dynamics of the nuclear spin can be reduced to

$$\rho_I(T_{\rm tot}) = \frac{1}{2}\begin{matrix}|\uparrow\rangle \\ |\downarrow\rangle\end{matrix}\begin{pmatrix}1+\mathcal{P}(T_{\rm tot}) & 0 \\ 0 & 1-\mathcal{P}(T_{\rm tot})\end{pmatrix}, \tag{B12}$$

where $\mathcal{P}(t) = |\beta(t)|^2 = \sin^2(\theta_p)\sin^2(\Omega_r t/2)$. This density matrix can be represented in the Pauli basis as $\rho(t) = [\mathbb{I} + \mathcal{P}(t)\hat{\sigma}_z]/2$. The polarization, defined as $\langle\hat{\sigma}_z(t)\rangle/2 = {\rm tr}[\rho(t)\hat{\sigma}_z]/2$, is found to be

$$\langle\hat{I}_z(T_{\rm tot} = 2N_pT)\rangle = \frac{\mathcal{P}(T_{\rm tot})}{2} = \frac{1}{2}\sin^2(\theta_p)\sin^2\left(\Omega_r N_p T\right), \tag{B13}$$

and completely equivalent to the result of the previous section.

However, in the experiment, the NV is repeatedly optically reinitialized into the $m_s = 0$ state, with a repetition number R. All single-spin simulations saturate to an asymptotic envelope as $R \to \infty$, although the rate at which the limit is approached differs significantly, as illustrated in Fig. 5. Weaker spins evidently polarize more slowly, even in the isolated spin case. In addition, there are the many-body effects, such as dark-state formation and the "spin blocking" that we investigated here that can significantly reduce the polarization rate.

Even in the single-spin case, both the simulated and experimental polarization traces show a detailed structure of "polarization dips." In the following sections, we analyze a key mechanism which causes sharp polarization dips, prior to discussing many-spin effects.

2. Polarization envelope side dips

In Fig. 5 and other figures, one sees extremely large "side dips," symmetrically distributed about the resonant T_r where the average Hamiltonian model predicts zero polarization, but full numerics allow even negative polarization.

Within the average Hamiltonian model, the polarization in Eq. (B13) is zero when the condition

$$\sin(\Omega_r N_p T) = 0 \tag{B14}$$

is met. Solving this equation for T yields the position for a series of such side dips, $T_{\rm dip}$, to be

$$T_{\rm dip} = \frac{T_r}{(1+\mu^2)}\left[1 \pm \frac{n}{kN_p}\sqrt{1+\mu^2\left(\frac{k^2N_p^2}{n^2}-1\right)}\right]$$
$$\simeq T_r\left[1 \pm \frac{n}{kN_p}\right], \tag{B15}$$

where $n \in \mathbb{Z}^+$, $n > 0$ is the nth side dip.

Here, k is the resonance harmonic and $T_r = k\pi/\omega_I$, while $\mu = 2g/\omega_I$. For harmonic $k = 3$, the side dips are approximately

$$T_{\rm dip} \simeq T_r\left(1 \pm \frac{n}{3N_p}\right), \tag{B16}$$

assuming $\mu \ll 1$ since the nuclear spins and magnetic field used here are $g \ll \omega_I$.

APPENDIX C: TWO-SPIN POLARIZATION

The average Hamiltonian for the two-spin system is a straightforward extension of the single-spin case,

$$\hat{H}_{\rm avg} = g_1(\hat{S}_+\hat{I}_-^{(1)} + \hat{S}_-\hat{I}_+^{(1)}) + \delta_1\hat{I}_z^{(1)} + g_2(\hat{S}_+\hat{I}_-^{(2)} + \hat{S}_-\hat{I}_+^{(2)}) + \delta_2\hat{I}_z^{(2)}, \tag{C1}$$

and corresponds to an 8×8 matrix that may be decomposed into four independent subspaces. As with the single-spin model, the stretched states $|\uparrow\uparrow\uparrow\rangle$ and $|\downarrow\downarrow\downarrow\rangle$ are eigenstates of $\hat{H}_{\rm avg}$, with

$$|\Phi_1\rangle = |\uparrow\uparrow\uparrow\rangle, \quad \epsilon_1 = \frac{\delta_1+\delta_2}{2} = \frac{\delta_+}{2}, \tag{C2}$$

$$|\Phi_2\rangle = |\downarrow\downarrow\downarrow\rangle, \quad \epsilon_2 = -\frac{\delta_1+\delta_2}{2} = -\frac{\delta_+}{2}. \tag{C3}$$

The remaining states form two decoupled subspaces of $\{|\uparrow\downarrow\uparrow\rangle, |\downarrow\uparrow\uparrow\rangle, |\uparrow\uparrow\downarrow\rangle\}$ with overall magnetization $M_j = 1/2$ and $\{|\downarrow\downarrow\uparrow\rangle, |\uparrow\downarrow\downarrow\rangle, |\downarrow\uparrow\downarrow\rangle\}$ with overall magnetization $M_j = -1/2$. For the case of the $M_j = 1/2$ subspace, the

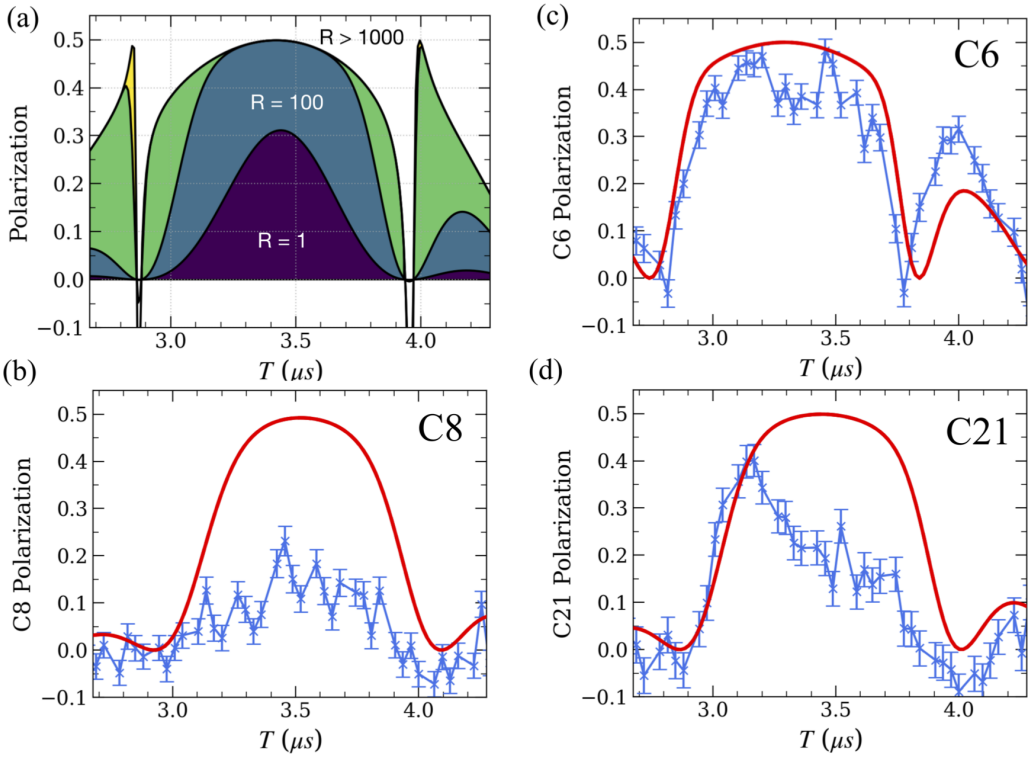

FIG. 5. (a) Simulation showing that with increasing repetitions R of the polarization sequence, in principle, all spins tend to an asymptotic polarization envelope. Isolated strong spins attain the $R \to \infty$ limit for $R \sim 10$, while isolated very weak-coupled spins may require $R \gg 1000$. Comparisons of single-spin simulations of polarization (red) to experimental data (blue) for three weak-coupled spins in a cluster (b) C6, (c) C8, and (d) C21. The parameters used here are $R = 1000$ and $N_p = 2$. The modest-coupling strength C6 is close to asymptotic. The weak-coupled spins C8 and C21 are far from the limit, not only because of the weak coupling, but also because of the many-body spin blocking investigated here.

Hamiltonian matrix takes the form

$$\hat{H}_{\rm avg} = \begin{matrix} \\ |\uparrow\downarrow\uparrow\rangle \\ |\downarrow\uparrow\uparrow\rangle \\ |\uparrow\uparrow\downarrow\rangle \end{matrix} \begin{matrix} \begin{matrix} |\uparrow\downarrow\uparrow\rangle & |\downarrow\uparrow\uparrow\rangle & |\uparrow\uparrow\downarrow\rangle \end{matrix} \\ \begin{pmatrix} -\delta_-/2 & g_1 & 0 \\ g_1 & \delta_+/2 & g_2 \\ 0 & g_2 & \delta_-/2 \end{pmatrix} \end{matrix}, \tag{C4}$$

where $\delta_- = \delta_1 - \delta_2$.

1. Dark and Bright States

For the degenerate on-resonant nuclear detuning case, $\delta_1 = \delta_2 = 0$,

$$\hat{H}_{\rm avg} \equiv \begin{matrix} \\ |\uparrow\downarrow\uparrow\rangle \\ |\downarrow\uparrow\uparrow\rangle \\ |\uparrow\uparrow\downarrow\rangle \end{matrix} \begin{matrix} \begin{matrix} |\uparrow\downarrow\uparrow\rangle & |\downarrow\uparrow\uparrow\rangle & |\uparrow\uparrow\downarrow\rangle \end{matrix} \\ \begin{pmatrix} 0 & g_1 & 0 \\ g_1 & 0 & g_2 \\ 0 & g_2 & 0 \end{pmatrix} \end{matrix}. \tag{C5}$$

There are well-studied eigenstates,

$$\begin{aligned} |\psi_{B_-}\rangle &= |\uparrow\rangle_{\rm NV}[\cos\varphi|\downarrow\uparrow\rangle + \sin\varphi|\uparrow\downarrow\rangle - |\downarrow\uparrow\uparrow\rangle], \\ |\psi_{B_+}\rangle &= |\uparrow\rangle_{\rm NV}[\cos\varphi|\downarrow\uparrow\rangle + \sin\varphi|\uparrow\downarrow\rangle + |\downarrow\uparrow\uparrow\rangle], \\ |\psi_D\rangle &= |\uparrow\rangle_{\rm NV}[\cos\varphi|\uparrow\downarrow\rangle - \sin\varphi|\downarrow\uparrow\rangle], \end{aligned} \tag{C6}$$

where $|\psi_D\rangle$ is termed a "dark state," with eigenvalue $\epsilon = 0$, and $|\psi_{B_\pm}\rangle$ the so-called bright states with $\epsilon_\pm = \pm g_{\rm rms}/2 = \sqrt{g_1^2 + g_2^2}/2$, defining $\cos\varphi = g_1/g_{\rm rms}$, $\sin\varphi = g_2/g_{\rm rms}$.

The dark state $|\psi_D\rangle$ has no overlap with the fully polarized state $|\downarrow\uparrow\uparrow\rangle$, and thus any state that acquires a significant dark-state component may not polarize. For the bright states, the converse is true. For the case $g_1 = g_2 = g$, the problem is even simpler as the matrix reduces to $g\hat{S}_x$, the spin-1 angular momentum x matrix.

However, we need to consider the behavior in the presence of detuning, hence away from resonance, as well as spins that are not perfectly degenerate. Neither the uncoupled Zeeman states nor the dark-bright states are eigenstates of the general $\hat{H}_{\rm avg}$ case. For insight, we represent $\hat{H}_{\rm avg}$ in a slightly modified alternative "dark-bright" basis $\{|\psi_{\rm pol}\rangle, |\psi_B^{(1)}\rangle, |\psi_D^{(1)}\rangle\}$, where

$$|\psi_{\rm pol}\rangle = |\downarrow\uparrow\uparrow\rangle, \tag{C7}$$

$$|\psi_B^{(1)}\rangle = |\uparrow\rangle_{\rm NV}[\cos\varphi|\downarrow\uparrow\rangle + \sin\varphi|\uparrow\downarrow\rangle], \tag{C8}$$

$$|\psi_D^{(1)}\rangle = |\uparrow\rangle_{\rm NV}[\cos\varphi|\uparrow\downarrow\rangle - \sin\varphi|\downarrow\uparrow\rangle], \tag{C9}$$

for $\tan\varphi = g_2/g_1$. In this basis,

$$\hat{H}'_{\rm avg} = \begin{matrix} \\ |\psi_{\rm pol}\rangle \\ |\psi_B^{(1)}\rangle \\ |\psi_D^{(1)}\rangle \end{matrix} \begin{matrix} \begin{matrix} |\psi_{\rm pol}\rangle & |\psi_B^{(1)}\rangle & |\psi_D^{(1)}\rangle \end{matrix} \\ \begin{pmatrix} \delta_+/2 & g_{\rm rms} & 0 \\ g_{\rm rms} & -\delta_-\cos(2\varphi)/2 & \delta_-\sin(2\varphi)/2 \\ 0 & \delta_-\sin(2\varphi)/2 & \delta_-\cos(2\varphi)/2 \end{pmatrix} \end{matrix} \tag{C10}$$

that we use to analyze two important cases.

2. Dark-Bright States in the Presence of Detuning

First we consider the case where the two nuclear spins are degenerate ($A_z^{(1)} = A_z^{(2)}$) so $\delta_- = 0$ and $\delta_+ = 2\delta_1 = 2\delta$, a

detuning which varies as the experiment sweeps T through the resonance $T = T_r$. In practice, we require $|\delta_-| \ll g_{\rm rms}$. The dark state $|\psi_D^{(1)}\rangle$ decouples from the other bright states. The other two states form a separate subspace $\{|\psi_{\rm pol}\rangle|\psi_B^{(1)}\rangle\}$, such that the Hamiltonian is $\hat{H} = \delta/2\mathbb{I} + \delta\hat{I}_z + 2g_{\rm rms}\hat{I}_x$. This Hamiltonian is similar to the single-spin model with $g \to g_{\rm rms}$ and an extra global energy shift. Hence,

$$|\Phi_+^{(1)}\rangle = \cos\left(\frac{\theta}{2}\right)|\psi_{\rm pol}\rangle + \sin\left(\frac{\theta}{2}\right)|\psi_B^{(1)}\rangle, \quad \epsilon_+^{(1)} = \frac{\delta+\omega}{2},$$
$$|\Phi_-^{(1)}\rangle = \sin\left(\frac{\theta}{2}\right)|\psi_{\rm pol}\rangle - \cos\left(\frac{\theta}{2}\right)|\psi_B^{(1)}\rangle, \quad \epsilon_-^{(1)} = \frac{\delta-\omega}{2},$$
$$\left|\Phi_D^{(1)}\right\rangle = \left|\psi_D^{(1)}\right\rangle, \quad \epsilon_0 = 0, \tag{C11}$$

where $\tan\theta = 2g_{\rm rms}/\delta$ and $\omega = \sqrt{\delta^2 + 4g_{\rm rms}^2}$ are dependent on the detuning. The dark state is δ independent and is fully decoupled (effective zero coupling to the polarization state), even for $g_1 = g_2$. As δ is varied, $|\Phi_\pm^{(1)}\rangle$ sweep through a single avoided crossing with enhanced coupling $g_{\rm rms}$.

If we take the initial state of the system to be $|\uparrow\rangle$ for the NV and an initial state $|\psi(0)\rangle = |\uparrow\downarrow\uparrow\rangle$, temporal evolution will yield

$$|\psi(T_{\rm tot})\rangle = e^{-i\delta T_{\rm tot}/2}\cos\varphi\left[\alpha(T_{\rm tot})\left|\psi_B^{(1)}\right\rangle + \beta(T_{\rm tot})|\psi_{\rm pol}\rangle\right] - \sin\varphi\left|\psi_D^{(1)}\right\rangle, \tag{C12}$$

where $\alpha(t) = \cos(\omega t/2) + i\cos(\theta)\sin(\omega t/2)$, $\beta(t) = -i\sin(\theta)\sin(\omega t/2)$, and $\cos\varphi = g_1/g_{\rm rms}$. This is similar to a single spin only with an extra, time-independent term involving the dark state. The population of the state in the polarized state is then

$$P_{\rm pol}(T_{\rm tot} = 2N_pT) = \cos^2\varphi\sin^2\theta\sin^2(\omega N_pT). \tag{C13}$$

This population has the same off-resonance envelope with $\sin\theta$ blocking population transfer if $\delta \neq 0$, but also has an extra term involving φ, which quantifies overlap with the dark state and suppresses population transfer to the polarized state, as $\cos^2\varphi \leqslant 1$. This is seen in Eq. (C13) at arbitrary $\delta(\tau)$. An equivalent approach can be used to analyze the $M_j = -1/2$ subspace $\{|\downarrow\downarrow\uparrow\rangle, |\uparrow\downarrow\downarrow\rangle, |\downarrow\uparrow\downarrow\rangle\}$.

In summary, for degenerate spins, dark states cause a proportion of the spin's population to remain unpolarized, even for a large number of repetitions R. Perfect degeneracy is not typical in a realistic setting, and in most cases slow mixing between dark and bright states allows slow polarization. An example of dark-state polarization suppression is shown in Fig. 6 between C8 and C4, which are almost degenerate, as in Table I. There is a significant reduction in polarization between the single-spin simulation of C8 and a two-spin simulation with only C8 and C4, which better captures the experimental behavior.

3. Spin Blockade

In this section, we present the details of the spin-blocking effect which is introduced in this work. We consider the case of anisotropic coupling strengths $g_1 \gg g_2$. We relabel $g_1 \equiv G$ and $g_2 \equiv g$, and hence $G \gg g$, to clearly distinguish the strong- from the weak-coupling spin. However, the spins are not fully degenerate or $\delta_- \neq 0$, but we assume $|\delta_-| \ll G$. Such a scenario may be common when using NV centers to polarize a cluster of distant nuclear spins. There is typically a small number of proximate or near-proximate

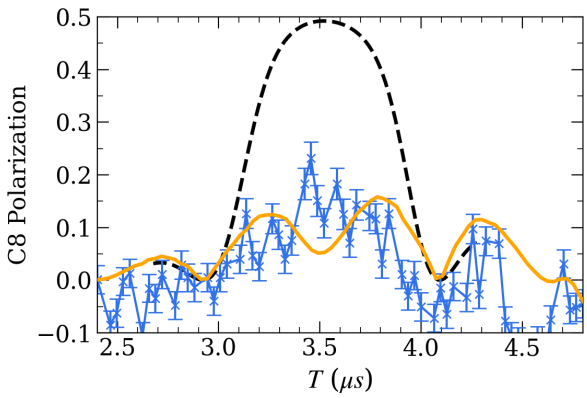

FIG. 6. Illustration of polarization saturation for spin C8 due to spin-pair dark states formed with a nearly degenerate spin C4. Simulations of single spin C8 (dashed line) are shown to fully polarize after $R = 1000$ of PulsePol with $N_p = 2$. This is not seen in experiment (blue), which only reaches a polarization of 0.2. This experimental saturation is reproduced to good effect by simulation of the spin pair C8 and C4 (orange).

TABLE I. List of parallel and perpendicular couplings between the ^{13}C spins and the NV. In [21], the same spins are labeled under a different numbering; the numbering system is included in the table for consistency.

Label	$A_z/2\pi$ (kHz)	$A_x/2\pi$ (kHz)	$\omega_I^{(i)}$ (rad/μs)	M Label
C0	213.153	3	2.04	C9
C1	−36.308	26.62	2.83	C18
C2	20.569	41.51	2.65	C12
C3	−11.346	59.21	2.75	C5
C4	8.029	21.0	2.69	C13
C5	24.399	24.81	2.64	C19
C6	−48.58	9.0	2.86	C6
C7	14.58	10	2.67	C11
C8	7.683	4	2.69	C22
C9	−20.72	12	2.78	C1
C10	−23.22	13	2.78	C2
C11	−13.961	9	2.75	C15
C12	−31.25	8	2.81	C3
C13	−14.07	13	2.76	C4
C15	−5.62	5	2.73	C17
C16	−19.815	5.3	2.77	C14
C17	−4.66	7	2.73	C16
C18	17.643	8.6	2.66	C10
C20	−8.32	3	2.74	C7
C21	−9.79	5.0	2.74	C8
C22	1.212	13	2.71	C21
C23	2.69	11	2.70	C20
C24	−3.177	2	2.72	C23
C25	−4.039	0.5	2.72	C27
C26	−4.225	0.771	2.72	C24
C27	−3.873	1.247	2.72	C25
C28	−3.618	9.472	2.72	C26

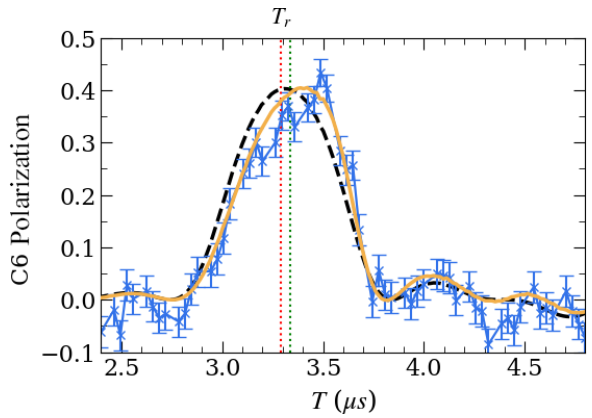

FIG. 7. Polarization of C6 displaced by blocking spin C3. Simulations of C6 polarization with C3 (orange line) after $R = 100$ of PulsePol with $N_p = 2$ have a slightly displaced polarization peak from the single C6 spin (dashed black line) despite having a stronger perpendicular coupling of $A_x = 7.68$ kHz $\times 2\pi$. This displacement is seen in the experimental data for C6 polarization (blue).

spins such as spin C3 where this condition is satisfied by a larger number of weaker-coupled spins such as C16, C21, C25, etc. The anisotropy requirement is not too stringent: blockade spins can displace the resonance of "local" spins with moderate perpendicular coupling, an effect which may need to be considered when using local clusters as memory registers. Figure 7 demonstrates an example: spin C6 has reasonable coupling $A_x/(2\pi) = 9$ kHz, but still experiences a small resonance shift from blockade spin C3, suggesting that the blocking effect is quite common.

For this case, we write the effective Hamiltonian in Eq. (C4) $\hat{H}_{\rm avg} = \hat{H}_0 + \hat{V}$ as a zeroth-order Hamiltonian plus perturbation matrix, where

$$\hat{H}_0 + \hat{V} = \begin{matrix} \\ |\uparrow\downarrow\uparrow\rangle \\ |\downarrow\uparrow\uparrow\rangle \\ |\uparrow\uparrow\downarrow\rangle \end{matrix} \begin{matrix} \begin{matrix} \quad & \quad & \quad \end{matrix} \\ \begin{pmatrix} -\delta_-/2 & G & 0 \\ G & \delta_+/2 & 0 \\ 0 & 0 & \delta_-/2 \end{pmatrix} \end{matrix} + \begin{pmatrix} 0 & 0 & 0 \\ 0 & 0 & g \\ 0 & g & 0 \end{pmatrix}. \tag{C14}$$

The detunings are relabeled to $\delta_1 \to \delta_B$ and $\delta_2 \to \delta_s$ for a blockade spin and "small" spin, respectively. The unperturbed Hamiltonian $\hat{H}_0$ can be reduced into two subspaces. One subspace only contains the state $\{|\uparrow\uparrow\downarrow\rangle\}$ which decouples from the others. Therefore, the eigenstate and eigenvalue can be read from the matrix to be $|\Phi_3^{(0)}\rangle = |\uparrow\uparrow\downarrow\rangle$, $\epsilon_3^{(0)} = \delta_-/2$. The remaining states form their own subspace $\{|\uparrow\downarrow\uparrow\rangle, |\downarrow\uparrow\uparrow\rangle\}$ with Hamiltonian

$$\hat{\tilde{H}}_0 = \begin{matrix} \\ |\downarrow\uparrow\uparrow\rangle \\ |\uparrow\downarrow\uparrow\rangle \end{matrix} \begin{matrix} \begin{matrix} \quad & \quad \end{matrix} \\ \begin{pmatrix} \delta_+/2 & G \\ G & -\delta_-/2 \end{pmatrix} \end{matrix} = \frac{\delta_s}{2}\mathbb{I} + \delta_B \hat{I}_z + 2G\hat{I}_x. \tag{C15}$$

As expected, this takes the same form as the single-spin case with an extra global energy term from the second spin. The corresponding eigenstates and eigenvalues are

$$\begin{aligned} |\Phi_1^{(0)}\rangle &= \cos\left(\frac{\theta_p}{2}\right)|\downarrow\uparrow\uparrow\rangle + \sin\left(\frac{\theta_p}{2}\right)|\uparrow\downarrow\uparrow\rangle, \\ \epsilon_1^{(0)} &= \frac{\delta_s + \omega}{2}, \\ |\Phi_2^{(0)}\rangle &= \sin\left(\frac{\theta_p}{2}\right)|\downarrow\uparrow\uparrow\rangle - \cos\left(\frac{\theta_p}{2}\right)|\uparrow\downarrow\uparrow\rangle, \\ \epsilon_2^{(0)} &= \frac{\delta_s - \omega}{2}, \\ |\Phi_3^{(0)}\rangle &= |\uparrow\uparrow\downarrow\rangle, \quad \epsilon_3^{(0)} = \frac{\delta_-}{2}, \end{aligned} \tag{C16}$$

where $\omega = \sqrt{\delta_B^2 + 4G^2}$ and $\tan\theta_p = 2G/\delta_B$. The superscript (0) is used to denote that these are the unperturbed eigenstates and eigenvalues of $\hat{H}_0$. In the basis of $\hat{H}_0$ eigenstates, the full Hamiltonian is $\hat{H}'_{\rm avg} = \hat{H}'_0 + \hat{V}'$, with

$$\hat{H}'_0 = \begin{matrix} |\Phi_1^{(0)}\rangle \\ |\Phi_2^{(0)}\rangle \\ |\Phi_3^{(0)}\rangle \end{matrix} \begin{matrix} \begin{matrix} \quad & \quad & \quad \end{matrix} \\ \begin{pmatrix} (\delta_s+\omega)/2 & 0 & 0 \\ 0 & (\delta_s-\omega)/2 & 0 \\ 0 & 0 & \delta_-/2 \end{pmatrix} \end{matrix}, \tag{C17}$$

and the perturbation

$$\hat{V}' = \begin{pmatrix} 0 & 0 & gc_p \\ 0 & 0 & gs_p \\ gc_p & gs_p & 0 \end{pmatrix}, \tag{C18}$$

where $s_p = \sin(\theta_p/2)$ and $c_p = \cos(\theta_p/2)$. For a 2×2 single-spin system, PulsePol is resonant with the spin when the eigenvalues of $\hat{H}_0$ are degenerate, allowing g to lift the degeneracy and couple the two eigenstates. Ignoring the blockade spin ($G = 0$), the resonance of the second spin occurs when $\delta_+ = \delta_-$, or $\delta_s = 0$. This is satisfied when the frequency of the PulsePol protocol ω_p is resonant with the spin's precession frequency, or

$$\omega_p = \omega_I^{(s)}. \tag{C19}$$

Using the definition of the protocol frequency $\omega_p = 3\pi/T$, the period of PulsePol, which is resonant with the nuclear spin, is $T_r = 3\pi/\omega_I^{(s)}$.

The same principle can be applied to the blockade spin system, where the degeneracy is lifted by the perturbation, $\hat{V}'$, when two eigenvalues of the 3×3 Hamiltonian $\hat{H}'_0$ are degenerate. Explicitly, $\hat{V}'$ weakly couples the state $|\Phi_3^{(0)}\rangle$ to either $|\Phi_1^{(0)}\rangle$ or $|\Phi_2^{(0)}\rangle$. The eigenvalues of $\hat{H}'_0$ are different depending on the sign of δ_-. For example, if $\delta_- < 0$, then the eigenvalues $\epsilon_1^{(0)}$ and $\epsilon_3^{(0)}$ are never degenerate, and $\hat{V}'$ is not strong enough to couple the corresponding states. However, there is a value of detuning in which $\epsilon_2^{(0)} = \epsilon_3^{(0)}$, giving an updated condition for the weaker spin's resonance. For $\delta_- > 0$, this is reversed and, instead, $\epsilon_1^{(0)} = \epsilon_3^{(0)}$. We will only consider systems where $\delta_- < 0$, although the results are identical. The resonance satisfies $\delta_s - \sqrt{\delta_B^2 + 4G^2} = \delta_B - \delta_s$. Using the definition that $\delta_i = \omega_I^{(i)} - \omega_p$, then

$$\omega_p = \tilde{\omega}_I^{(s)} = \omega_I^{(s)} + \frac{G^2}{\delta_-}, \tag{C20}$$

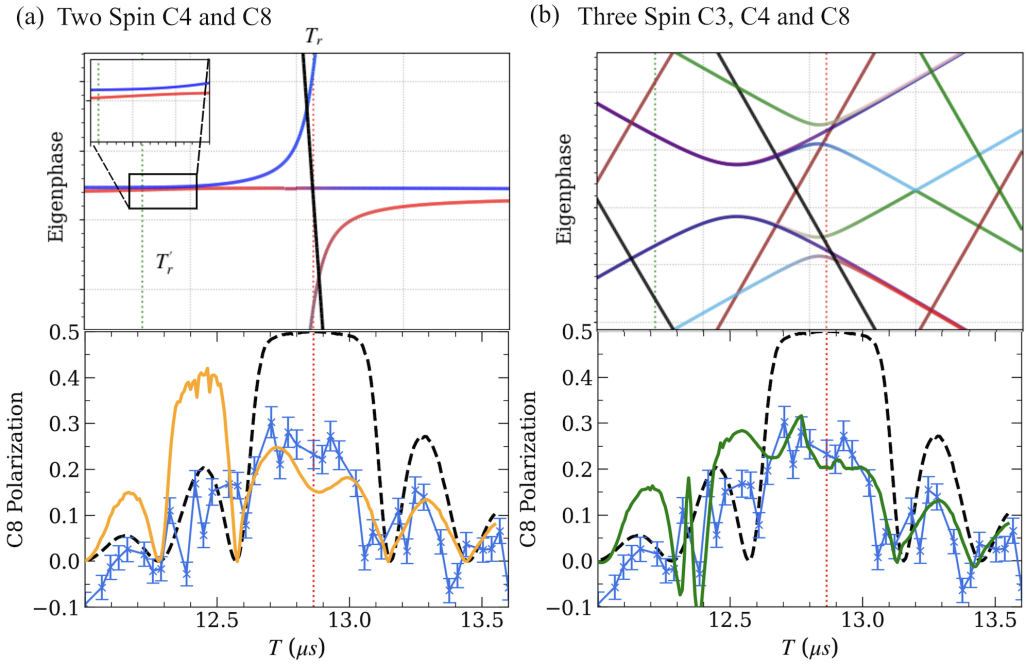

FIG. 8. Effect of two competing blockade spins: the polarization of C8 at a higher harmonic ($k = 11$). (a) The Floquet phases and polarization for a two-spin system of C4 and C8. A displaced avoided crossing for C8 is present in the Floquet phases and a corresponding displaced polarization peak from the single spin (black) to the two spin (orange). However, experimental data (blue) instead simply have significantly lower polarization. (b) Floquet phases and polarization for a three-spin system of C3, C4, and C8. The original displaced avoided crossing of C8 from (b) is now nearly degenerate with the avoided crossing of C3, which now acts as a blockade spin, pushing the crossing back towards its original position. This three-spin simulation (green) demonstrates the flattening of the two-spin peak and fits the experimental data better, showing the effect of higher-order multispin effects. Simulations and data here are for $R = 1000$ repetitions of $N_p = 4$ PulsePol cycles.

which is shifted by G^2/δ_- from the original single-spin resonant frequency $\omega_I^{(s)}$. Assuming that the coupling $g \ll G \ll \omega_L$, then the relative displacement of the resonant period is

$$\frac{\Delta T_r}{T_r} \simeq -\frac{G^2}{\omega_I^{(s)}\left(\omega_I^{(B)} - \omega_I^{(s)}\right)}, \tag{C21}$$

where the new resonance is at $T_r' \simeq T_r + \Delta T_r$. The robustness of Eq. (C21) is tested against both two-spin simulations and experimental polarization of C21 in Fig. 3 of the main paper.

Furthermore, degenerate perturbation theory can be used to find the Rabi frequency of this resonance by solving the 2×2 matrix in the subspace $\{|\Phi_2^{(0)}\rangle, |\Phi_3^{(0)}\rangle\}$, which is of the form $\hat{\tilde{H}}' = \epsilon\mathbb{I} + 2gs_p\hat{I}_x$, where $\epsilon = \epsilon_2^{(0)} = \epsilon_3^{(0)}$. The corresponding Rabi frequency is found to be

$$\Omega_r \simeq 2g \sin\left(\frac{\theta_p}{2}\right). \tag{C22}$$

This Rabi frequency is attenuated by a factor $\sin\theta/2$ relative to the one-spin case. In fact, if $|\Delta T_r/T_r| \gg 1$, then the coupling between the two states will be completely suppressed and $\Omega_r = 0$. However, for the typical scenarios studied here, the displacement is less drastic and $\Omega_r \sim 2g$. We note that in the $\delta_- \to 0$ limit, the shift tends to infinity. In this scenario, the second small crossing vanishes and the dark-mode behavior is regained.

4. Competing Blockade Spins

While the focus here was primarily on the case of a single spin (e.g., C3), simultaneously and independently blocking multiple weaker-coupled spins, we can consider the case where two blockade spins affect the same weaker-coupled spin. This results in a competing or combined blockade effect. Such a scenario is identifiable in the experimental cluster here, when looking at higher harmonic resonances of PulsePol at larger T.

In previous sections, a PulsePol resonance of harmonic $k = 3$ was studied. Consider now a higher harmonic, $k = 11$, at a much greater periodicity T. At higher harmonics, single-spin resonances have a greater spacing, meaning that C8 and C4 are relatively close but no longer degenerate. Hence, the polarization of C8 no longer saturates due to dark states and is displaced by $\Delta T_r \simeq -0.64$ μs. A simulation of this higher harmonic displacement of C8 due to C4 is shown in the first panel of Fig. 8. However, this is not seen in the experimental data, where there is significantly less polarization than expected in this region of T. In fact, by considering the initial blockade spin C3 in simulations, as is done in the second panel of Fig. 8, polarization levels closer to the experimental data are obtained.

As in the Floquet states in Fig. 8, the expected displacement of the avoided crossing for C8 due to blockade spin C4 is nearly degenerate with the avoided crossing of C3, which was previously shown to act as a blockade spin for others with small A_x. Therefore, this shift closer to C3 causes a

secondary blockade effect on C8, displacing the resonance back towards its original position and "smearing" the polarization across T. This double-blockade effect on C8 is a three-spin effect, further highlighting the importance of considering many-body effects when performing polarization of clusters.

[1] R. Schirhagl, K. Chang, M. Loretz, and C. L. Degen, Nitrogen-vacancy centers in diamond: Nanoscale sensors for physics and biology, Annu. Rev. Phys. Chem. **65**, 83 (2014).

[2] F. Shi, X. Kong, P. Wang, F. Kong, N. Zhao, R.-B. Liu, and J. Du, Sensing and atomic-scale structure analysis of single nuclear-spin clusters in diamond, Nat. Phys. **10**, 21 (2014).

[3] N. Zhao, J. L. Hu, S. W. Ho, J. T. K. Wan, and R-B. Liu, Atomic-scale magnetometry of distant nuclear spin clusters via nitrogen-vacancy spin in diamond, Nat. Nanotechnol. **6**, 242 (2011).

[4] N. Zhao, J. Honert, B. Schmid, M. Klas, J. Isoya, M. Markham, D. Twitchen, F. Jelezko, R.-B. Liu, H. Fedder, and J. Wrachtrup, Sensing single remote nuclear spins, Nat. Nanotechnol. **7**, 657 (2012).

[5] N. Bar-Gill, L. M. Pham, A. Jarmola, D. Budker, and R. L. Walsworth, Solid-state electronic spin coherence time approaching one second, Nat. Commun. **4**, 1743 (2013).

[6] P. Cappellaro, L. Jiang, J. S. Hodges, and M. D. Lukin, Coherence and control of quantum registers based on electronic spin in a nuclear spin bath, Phys. Rev. Lett. **102**, 210502 (2009).

[7] P. Neumann, R. Kolesov, B. Naydenov, J. Beck, F. Rempp, M. Steiner, V. Jacques, G. Balasubramanian, M. L. Markham, D. J. Twitchen, S. Pezzagna, J. Meijer, J. Twamley, F. Jelezko and J. Wrachtrup, Quantum register based on coupled electron spins in a room-temperature solid, Nat. Phys. **6**, 249 (2010).

[8] H. Bernien, B. Hensen, W. Pfaff, G. Koolstra, M. S. Blok, L. Robledo, T. H. Taminiau, M. Markham, D. J. Twitchen, L. Childress, and R. Hanson, Heralded entanglement between solid-state qubits separated by three metres, Nature (London) **497**, 86 (2013).

[9] T. H. Taminiau, J. Cramer, T. van der Sar, V. V. Dobrovitski, and R. Hanson, Universal control and error correction in multiqubit spin registers in diamond, Nat. Nanotechnol. **9**, 171 (2014).

[10] G. Arrad, Y. Vinkler, D. Aharonov, and A. Retzker, Increasing sensing resolution with error correction, Phys. Rev. Lett. **112**, 150801 (2014)

[11] C. E. Bradley, J. Randall, M. H. Abobeih, R. C. Berrevoets, M. J. Degen, M. A. Bakker, M. Markham, D. J. Twitchen, and T. H. Taminiau, A ten-qubit solid-state spin register with quantum memory up to one minute, Phys. Rev. X **9**, 031045 (2019).

[12] N. Aslam, M. Pfender, P. Neumann, R. Reuter, A. Zappe, F. F. de Oliveira, A. Denisenko, H. Sumiya, S. Onoda, J. Isoya, and J. Wrachtrup, Nanoscale nuclear magnetic resonance with chemical resolution, Science **357**, 67 (2017).

[13] O. Sahin, E. de Leon Sanchez, S. Conti, A. Akkiraju, P. Reshetikhin, E. Druga, A. Aggarwal, B. Gilbert, S. Bhave, and A. Ajoy, High field magnetometry with hyperpolarized nuclear spins, Nat. Commun. **13**, 5486 (2022).

[14] A. Abragam and M. Goldman, Principles of dynamic nuclear polarisation, Rep. Prog. Phys. **41**, 395 (1978).

[15] I. Schwartz, J. Scheuer, B. Tratzmiller, S. Muller, Q. Chen, I. Dhand, Z.-Y. Wang, C. Muller, B. Naydenov, F. Jelezko, and M. B. Plenio, Robust optical polarization of nuclear spin baths using Hamiltonian engineering of nitrogen-vacancy center, Sci. Adv. **4**, eaat8978 (2018).

[16] J. E. Lang, J.-P. Tetienne, and T. S. Monteiro, Dynamical decoupling protocols with nuclear spin state selectivity, arXiv:1810.00174; J. E. Lang, D. A. Broadway, G. A. L. White, L. T. Hall, A. Stacey, L. C. L. Hollenberg, T. S. Monteiro, and J.-P. Tetienne, Quantum bath control with nuclear spin state selectivity via pulse-adjusted dynamical decoupling, Phys. Rev. Lett **123**, 210401 (2019).

[17] A. J. Healey, L. T. Hall, G. A. L. White, T. Teraji, M.-A. Sani, F. Separovic, J.-P. Tetienne, and L. C. L. Hollenberg, Polarization transfer to external nuclear spins using ensembles of nitrogen-vacancy centers, Phys. Rev. Appl. **15**, 054052 (2021).

[18] E. Urban, T. A. Johnson, T. Henage, L. Isenhower, D. D. Yavuz, T. G. Walker, and M. Saffman, Observation of Rydberg blockade between two atoms, Nat. Phys. **5**, 110 (2009).

[19] T. Villazon, A. Chandran, and P. W. Claeys, Integrability and dark states in an anisotropic central spin model, Phys. Rev. Res. **2**, 032052(R) (2020).

[20] J. Randall, C. E. Bradley, F. van der Gronden, A. Galicia, M. H. Abobeih, M. Markham, D. J. Twitchen, F. Machado, N. Y. Yao, and T. H. Taminiau, Many-body-localized discrete time crystal with a programmable spin-based quantum simulator, Science **374**, 1474 (2021).

[21] M. H. Abobeih, J. Randall, C. E. Bradley, H. P. Bartling, M. A. Bakker, M. J. Degen, M. Markham, D. J. Twitchen, and T. H. Taminiau, Atomic-scale imaging of a 27-nuclear-spin cluster using a quantum sensor, Nature (London) **576**, 411 (2019).

[22] G. L. van de Stolpe, D. P. Kwiatkowski, C. E. Bradley, J. Randall, S. A. Breitweiser, L. C. Bassett, M. Markham, D. J. Twitchen, and T. H. Taminiau, Mapping a 50-spin-qubit network through correlated sensing, arXiv:2307.06939.

[23] A. Schweiger and G. Jeschke, *Principles of Pulse Electron Paramagnetic Resonance* (Oxford University Press, Oxford, 2001).

[24] A. Schmidt and S. Vega, The Floquet theory of nuclear magnetic resonance spectroscopy of single spins and dipolar coupled spin pairs in rotating solids, J. Chem. Phys. **96**, 2655 (1992); T. O. Levante, M. Baldus, B. H. Meier, and R. R. Ernst, Formalized quantum mechanical Floquet theory and its application to sample spinning in nuclear magnetic resonance, Mol. Phys. **86**, 1195 (1995).

[25] J. E. Lang, R. B. Liu, and T. S. Monteiro, Dynamical-decoupling-based quantum sensing: Floquet spectroscopy, Phys. Rev. X **5**, 041016 (2015).

[26] J. H. Shirley, Solution of the Schrodinger equation with a Hamiltonian periodic in time, Phys. Rev. **138**, B979 (1965).

[27] T. Villazon, P. W. Claeys, A. Polkovnikov, and A. Chandran, Shortcuts to dynamic polarization, Phys. Rev. B **103**, 075118 (2021).

[28] J. E. Lang, J. Casanova, Z.-Y. Wang, M. B. Plenio, and T. S. Monteiro, Enhanced resolution in nanoscale NMR via

quantum sensing with pulses of finite duration, Phys. Rev. Appl. **7**, 054009 (2017).

[29] O. T. Whaites, J. Randall, T. H. Taminiau, and T. S. Monteiro, Adiabatic dynamical-decoupling-based control of nuclear spin registers, Phys. Rev. Res. **4**, 013214 (2022).

[30] M. Loretz, J. M. Boss, T. Rosskopf, H. J. Mamin, D. Rugar, and C. L. Degen, Spurious harmonic response of multipulse quantum sensing sequences, Phys. Rev. X **5**, 021009 (2015).

[31] X. Zhang, C.-L. Zou, N. Zhu, F. Marquardt, L. Jiang, and H. X. Tang, Magnon dark modes and gradient memory, Nat. Comm. **6**, 8914 (2015).

[32] C. Dong, V. Fiore, M. C. Kuzyk, and H. Wang, Optomechanical dark mode, Science **338**, 1609 (2012).